

( $M_w = 70\,000$ , [Aldrich]) and poly(styrene sulfonate) (PSS,  $M_w = 500\,000$ , [Polysciences]), according to the procedure by Barker et al. [20]. The PSS layer was sandwiched between two PAH layers.

Tetramethylorthosilicate (TMOS, [Aldrich]) was hydrolyzed under acidic conditions (molar ratio of TMOS/HCl/H<sub>2</sub>O was 1:1:55.6) for 30 min. The hydrolyzed solution was diluted with H<sub>2</sub>O to a ratio of 1:100. The diluted solution was then introduced into a two-compartment chamber separated by the nanonozzle-array film. The reaction was carried out in the presence of a direct-current electric field (80 V m<sup>-1</sup>), with the cathode immersed in the chamber facing the sharp end and the anode facing the large end. In this arrangement, the direction of EOF was from the sharp end to the large end. The electroaction proceeded for 15 min, after which the nanonozzle array was taken out, rinsed thoroughly with water and dried.

Received: July 13, 2004  
Final version: January 12, 2005

- [1] O. B. Bakajin, T. A. J. Duke, C. F. Chou, S. S. Chan, R. H. Austin, E. C. Cox, *Phys. Rev. Lett.* **1998**, *81*, 2737.
- [2] L. J. Guo, X. Cheng, C. F. Chou, *Nanotechnology* **2004**, *15*, 469.
- [3] O. A. Saleh, L. L. Sohn, *Nanotechnology* **2003**, *14*, 37.
- [4] T. A. Desai, D. J. Hansford, M. Ferrari, *Biomol. Eng.* **2000**, *17*, 23.
- [5] T. A. Desai, D. J. Hansford, M. Ferrari, *J. Membr. Sci.* **1999**, *159*, 221.
- [6] S. Y. Chou, P. R. Krauss, P. J. Renstrom, *Science* **1996**, *272*, 85.
- [7] D. H. Pearson, R. J. Tonucci, *Science* **1995**, *270*, 68.
- [8] W. Chu, M. Ferrari, *Proc. SPIE-Int. Soc. Opt. Eng.* **1995**, 2593, 9.
- [9] C. K. Harnett, G. W. Coates, H. G. Craighead, *J. Vac. Sci. Technol. B* **2001**, *19*, 2842.
- [10] S. Wang, L. J. Lee, unpublished.
- [11] T. Pangaribuan, K. Yamada, S. Jiang, H. Ohsawa, M. Ohtsu, *Jpn. J. Appl. Phys., Part 2* **1992**, *31*, L1302.
- [12] P. Pantano, D. R. Walt, *Rev. Sci. Instrum.* **1997**, *68*, 1357.
- [13] B. A. F. Puygranic, P. Dawson, *Ultramicroscopy* **2000**, *83*, 235.
- [14] T. Thurn-Albrecht, J. Schotter, G. A. Kastle, N. Emley, T. S. Baugh, L. Krusin-Elbaum, K. Guarini, C. T. Black, M. T. Tuominen, T. P. Russell, *Science* **2000**, *290*, 2126.
- [15] T. Mizutani, H. Nagase, N. Fujiwara, H. Ogoshi, *Bull. Chem. Soc. Jpn.* **1998**, *71*, 2017.
- [16] S. V. Patwardhan, N. Mukherjee, S. J. Clarson, *Silicon Chem.* **2002**, *1*, 47.
- [17] I. A. Aksay, M. Tsai, S. Manne, I. Honma, N. Yao, L. Zhou, P. Fenster, P. M. Eisenberger, S. M. Gruner, *Science* **1996**, *273*, 892.
- [18] M. Tsai, N. Yao, E. K. Im, Y. Xia, G. M. Whitesides, I. A. Aksay, *Nature* **1997**, *390*, 674.
- [19] B. J. Tarasevich, P. C. Rieke, J. Lu, *Chem. Mater.* **1996**, *8*, 292.
- [20] S. L. R. Barker, M. J. Talov, H. Canavan, J. J. Hickman, L. E. Locascio, *Anal. Chem.* **2000**, *72*, 4899.

## ery Low Conductivity Threshold in Bulk Isotropic Single-Walled Carbon Nanotube–Epoxy Composites\*\*

By Mateusz C. Bryning, Mohammad F. Islam, James M. C. Kikkawa, and Arjun G. Yodanis\*

Conducting composites are typically made by embedding conductive particles in an otherwise insulating matrix. The resulting materials often exhibit percolation-like electrical conductivity<sup>[1]</sup> with a well-defined insulator–conductor transition point, as a function of filler concentration. Applications for these composites include static-charge dissipation,<sup>[2]</sup> radio-frequency shielding, and field-emission sources.<sup>[3,4]</sup> Recently, single-walled carbon nanotubes (SWNTs) have emerged as an attractive option for conductive composite materials. Their small size, large aspect ratio, and high conductivity make it possible to create conductive composites at very low filling concentrations and with smaller inhomogeneities than can be achieved with larger particles. Lower filling fractions imply smaller perturbations of bulk physical properties, such as strength and optical transparency, as well as lower cost. We describe here a simple procedure for making conductive SWNT–epoxy composites that result in exceptionally low threshold concentrations with minimal modification of the epoxy matrix material.

Thus far, studies on the conductivity of SWNT–polymer composites<sup>[5–24]</sup> have reported low thresholds at volume fractions ranging from<sup>[7]</sup>  $\sim 1 \times 10^{-4}$  to several percent,<sup>[10]</sup> in some cases outperforming current technologies. Many aspects of the problem, however, are poorly understood and optimization remains elusive. The starting formulations of dispersed SWNTs frequently contain dense aggregates of nanotubes, as well as amorphous carbon and metallic impurities that can persist throughout processing and affect performance. Stabilizing the nanotubes in suspension can reduce aggregates, but introduces other problems. For example, covalent stabilization modifies the intrinsic SWNT conductivity, while steric stabilization can degrade contacts between nanotubes, and generally introduces additional impurities into the matrix. In addition, while well-dispersed SWNTs typically have a higher length-to-diameter ratio than aggregates, which is important for obtaining low thresholds,<sup>[25]</sup> interactions between particles also contribute to the formation of percolating networks. Network formation through particle chaining, in particular, can be a key factor in

\* Prof. A. G. Yodanis, M. C. Bryning, Dr. M. F. Islam, Prof. J. M. C. Kikkawa  
Department of Physics and Astronomy, University of Pennsylvania  
209 S. 33rd St., Philadelphia, PA 19104-6396 (USA)  
E-mail: yodanis@physics.upenn.edu

\*\* We gratefully acknowledge useful conversations about percolation with Brooks Harris, Tom Lubensky, and Brian DiDonna. This work is supported by grants from NSF (MRSE DMR0079909 (A.G., J.M.C.)) and DMR-0203378 (A.G.), NASA (NAG 21728 (A.G.)), and DARPA/ONR (N00015801808318). (M.C.).

lowering threshold concentrations. In carbon black composites, for example, the threshold can be lowered by inducing particle aggregation<sup>[26]</sup> and through the formation of diffuse, or “fluffy” agglomerates.<sup>[27]</sup> Long, flexible ropes of aligned multiwalled nanotubes (MWNTs) have also been used to make composites with threshold volume fractions as low as  $\sim 2 \times 10^{-5}$ , albeit with millimeter-scale inhomogeneities.<sup>[28]</sup> In such cases, as in all real composites, the relationship between particle aspect ratio and threshold concentration becomes difficult to predict. In SWNT composites these effects remain largely unexplored.

Here we show how the SWNT length/diameter aspect ratio and the spontaneous formation of nanotube networks affect the conductivity of bulk SWNT-epoxy composites. We compare two types of SWNTs with different mean aspect ratios, and introduce two nanotube-epoxy processing methods that inhibit or promote the formation of networks. We observe conductivity thresholds at SWNT volume fractions as low as  $5.2(+1.9/-0.5) \times 10^{-5}$ , nearly 10 times lower than values quoted in previous reports on SWNT composites in epoxy matrices.<sup>[5]</sup> All conductivity thresholds fall within the semi-dilute concentration regime of the rods, but the effect of nanotube aspect ratio on the threshold concentration is only marginally explained by simple models for rod percolation.

The key to this work is our starting formulation, a dilute (0.004 wt.-%), metastable dispersion of pure SWNTs in *N,N*-dimethylformamide (DMF). SWNTs remain well-dispersed in this suspension as isolated SWNTs and small SWNT bundles while under sonication (see Fig. 1g), but slowly reaggregate when sonication is turned off. The absence of stabilizing agents and formulation metastability permit networks to form prior to curing; the low SWNT concentration reduces aggregation, and so enables us to benefit from the high aspect ratio of isolated SWNTs. The samples were processed under a variety of sonication conditions, during which time the dilute SWNT/DMF solution was slowly added to the thermoset epoxy resin, and the DMF was allowed to evaporate. Continuous sonication produced more aggregated composites, while stopping of sonication prior to curing permitted networks to form. Taken together, the use of pristine SWNTs and sonication allowed us to produce fairly homogeneous composites with minimal perturbation of the high-strength epoxy. Interestingly, composites in which nanotubes were allowed to reaggregate exhibited lower thresholds, compared to more homogenized ones.

Laserfoven (Tubes@Rice) and HiPco (Carbon Nano-technologies, Inc) SWNTs were studied. The nanotubes were purified to a SWNT content of  $>95\%$ .<sup>[29]</sup> Atomic force microscopy (AFM) characterization showed that the laserfoven (HiPco) SWNTs had an average length,  $l = 516 \pm 286$  nm ( $167 \pm 90$  nm), and an average diameter,  $d = 1.35 \pm 0.15$  nm ( $1.1 \pm 0.3$  nm).<sup>[30]</sup> These dimensions cover the typical range of SWNT sizes available today. We found that adding the SWNT/DMF solution slowly in small discrete steps and allowing the DMF to evaporate between each step improved the effectiveness of the sonication. Sonication during processing

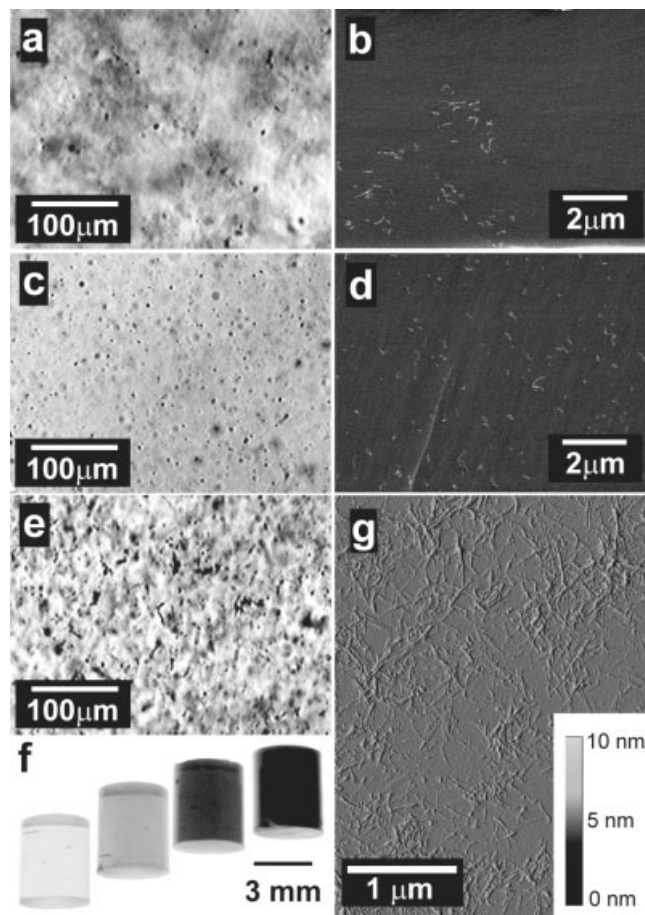


**Figure 1.** a)–e) Images of composites of SWNT volume fraction  $2.1 \times 10^{-4}$ . Information about SWNT distribution in the composites was obtained by using transmitted light microscopy (in  $\sim 300 \mu\text{m}$  slices) (a, c, e), and from scanning electron microscopy (SEM) of fractured surfaces (b, d). a) In a *sonicated* sample, dark and bright regions correspond to high and low SWNT concentrations, respectively. b) In SEM images of the same *sonicated* composite, SWNT ropes (white strips) appear in  $\sim 10 \mu\text{m}$  clusters on the surface. Here, the ropes are present only in the lower left quadrant of the field of view. c) In the more uniform gray color in this *sonicated* composite implies a more uniform SWNT distribution and in (a). d) SEM image of a *sonicated* sample shows that SWNT ropes are distributed more uniformly across the fractured surface than in (b). e) Dense aggregates are seen in a *sonicated* composite made from a more concentrated SWNT/DMF starting dispersion at 0.04 wt.-% (see text). f) Photographs of composites. SWNT volume fractions, from left to right, are  $2.6 \times 10^{-5}$ ,  $8.5 \times 10^{-5}$ ,  $8.1 \times 10^{-4}$ , and  $1.5 \times 10^{-4}$ . g) Tapping mode AFM image of a *sonicated* SWNTs adsorbed for over 30 min onto a hexamethylsilazane-treated silicon wafer from a well-sonicated, dilute DMF/SWNT suspension.

tends to break up transient SWNT networks and inhibit the formation of new ones. Once the desired SWNT concentration was reached in the sonicating resin as described above, an aliphatic amine crosslinker was stirred into the solution. At this stage, the samples were divided into two categories. In the first set, samples were placed into a hot water bath to cure at  $90^\circ\text{C}$  for 30 min; curing proceeded without sonication. Hereafter, we refer to these samples as “non-sonicated”. In the second set, samples were placed in the sonicator bath at  $80^\circ\text{C}$ ,

and were used under sonication for 30 min. We refer to these samples as “sonicured”. We found that “sonicured” samples were more homogeneous than “non-sonicured” ones, implying that SWNT networks that formed during sample processing were successfully dispersed.

A series of composite samples with increasing SWNT concentration is shown in Figure 1f. Our SWNT-epoxy composites exhibited a range of microscopic morphologies evident from optical microscopy of thin sections and SEM of fractured surfaces (see Fig. 1). An example of a “non-sonicured” sample is shown in Figures 1a, b. Reaggregation of SWNTs was clearly evident as bright and dark regions on the optical images. These diffuse aggregates were roughly 10 μm in diameter. SEM imaging confirmed that nanotube density varied on a similar length scale. Ropes of SWNTs were distributed in clusters on the fractured surfaces. These clusters were easily dispersed by continued sonication just prior to curing. An example of a aggregated “sonicured” sample is shown in Figures 1c, d. The optical and SEM images show that the SWNT distribution was quite homogeneous down to a few micrometers, and although some aggregates were present, their density was relatively low. We suspect the epoxy resin itself partially stabilizes the suspension<sup>[31]</sup> once the DMF evaporates, facilitating this dispersion. It is important to distinguish the diffuse features in our “non-sonicured” samples from dense aggregates, which result from a poor initial dispersion. For example, a sample made from a 0.04 wt.-% SWNT/DMF suspension, shown in Figure 1e, had a substantially larger number of dense aggregates, which presumably existed in the more concentrated starting suspensions and persisted throughout processing.

The electrical conductivity of the SWNT-epoxy composites was determined by two- and four-point contact dc-current (dc) conductivity measurements. Most of the measurements were obtained by the four-point method, in order to eliminate contact-resistance effects. Samples were prepared for the measurements as shown in the inset in Figure 2. The four-point current-voltage (*I-V*) curves were linear in the range studied, as shown in the same figure. In Figure 3, we show the conduc-

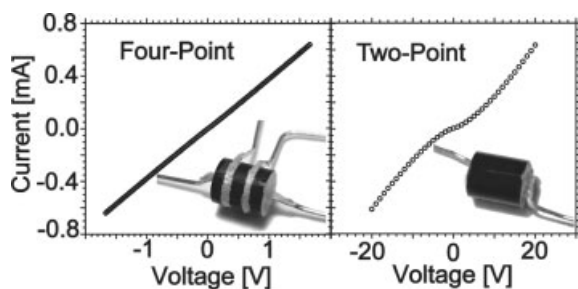


**Figure 2** Two-point and four-point *I-V* curves for a non-sonicured HiPco SWNT composite at  $8.6 \times 10^{-4}$  SWNT volume fraction showing typical response of our samples. The insets show composite samples mounted for two- and four-point conductivity measurements. At a given current, the measured voltage in the two-point measurement is significantly higher than that in the four-point, due to both contact resistance and a larger separation between the electrodes.

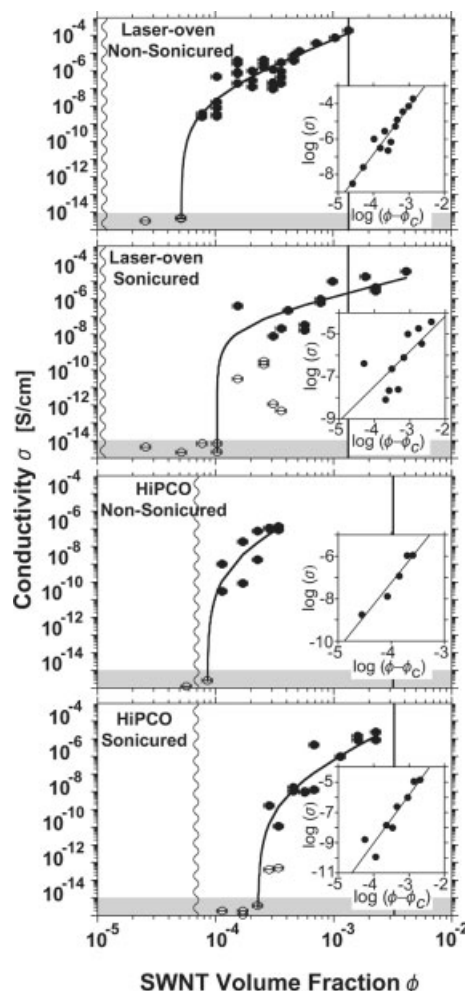


**Figure 3** Conductivity,  $\sigma$ , as a function of SWNT volume fraction,  $\phi$ , for non-sonicured and sonicured laser-oven and HiPco samples. The vertical lines in the charts indicate approximate transitions from dilute to semi-dilute regimes (wavy), and semi-dilute to concentrated regimes (solid). Each point in the plot represents a separately made composite. The observed scatter in conductivity is likely caused by small variations in processing conditions between samples. In contrast, the conductivities of different sections of the same sample were never more than 850% of each other. Filled circles represent four-point measurements. Open circles depict two-point alternating bias measurements. Points in shaded areas are below the baseline of our equipment. Connecting curves reflect the predicted behavior according to the best fits for the observed fresh-old,  $\phi$ , and the exponent,  $s$ . Insets show plots of  $\log(\sigma)$  as a function of  $\log(\phi - \phi_c)$  for the same data sets, where multiple points at the same concentration have been binned prior to fitting. Best-fit lines determining  $\phi_c$  and  $s$  are shown.

tivity,  $\sigma$ , of the non-sonicured and sonicured laser-oven and HiPco composites as a function of SWNT volume fraction,  $\phi$ . All four sets of composites exhibited a jump in the value of  $\sigma$  of 2 to 6 orders of magnitude over a small range in  $\phi$ , i.e., a percolation-like behavior. Near this threshold, we found  $\sigma \propto (\phi - \phi_c)^s$ ; thereafter we refer to  $\phi$  as the threshold volume fraction. To determine  $\phi_c$  and  $s$ , logarithms of the measured conductivity and volume fraction were compared to the equation  $\log(\sigma) = \log(C_0 + A(\phi - \phi_c)^s \Theta(\phi - \phi_c))$ , where  $C_0$  is the

constant background conductivity of the points below the threshold,  $\chi$  is a constant that depends on nanotube conductivity and network morphology, and  $\Theta(\phi - \phi_c)$  is the Heaviside step function, such that  $\Theta(x) = 0$  when  $x < 0$  and  $\Theta(x) = 1$  when  $x > 0$ . Two-point measurements above the threshold were excluded from the fits to avoid systematic errors due to contact resistance.

A least-squares analysis of the fits showed that  $\phi_c$  for each set of composites was strongly bounded by the regions between the highest insulating and lowest conducting points. The exponential fit, however, was not well bounded. The fit results for  $\phi_c$  and  $\beta$  are summarized in Table 1. Plots of  $\log(\sigma)$  versus  $\log(\phi - \phi_c)$  in the insets of Figure 3 show the conducting composite samples with best-fit lines whose slopes provide the best-fit exponent,  $\beta$ . The lowest measured threshold volume fraction was obtained for the non-sonicated laser-oven SWNTs; its value of  $5.2(+1.9/-0.5) \times 10^{-5}$  is approximately 10 times smaller than the lowest threshold concentration reported to date for SWNTs in epoxy.<sup>151</sup> Electrostatic dissipation applications typically require a conductivity of about  $10^{-5} \text{ Scm}^{-1}$ , which was reached when  $\phi \approx 5 \times 10^{-4}$  ( $\sigma \approx 10^{-4} \text{ Scm}^{-1}$  at  $\phi = 10^{-3}$ ). The magnitude of the conductivity is comparable to some results obtained for MWNTs in epoxy composites; note, however, that the length scale for inhomogeneity is  $\sim 10 \mu\text{m}$  or less for sonicated and non-sonicated samples (Fig. 1), compare with  $\sim 1 \text{ mm}$  in MWNT-epoxy samples.<sup>128</sup> Two other facts are clearly revealed in the data. First, the threshold is observed in the sonicated samples were higher (i.e., by  $\sim 2\times$ ) than the non-sonicated samples. Evidently, sonication disaggregated and homogenized SWNTs better just prior to curing, but the more reaggregated composites percolated more readily. Second, the laser-oven SWNT composites had approximately twofold lower thresholds than corresponding HiPco SWNT composites. This trend is qualitatively consistent with the expectations of simple models for percolation in random rod networks discussed below, which scale with rod length and diameter.

Since individual SWNTs behave somewhat like girders in solution,<sup>132</sup> it is useful to consider our observations in light of the predictions made by simple percolation models for isotropic dispersions of rod-like particles. Such dispersions can be classified by Doi-Edwards theory into dilute, semi-dilute, and concentrated regimes.<sup>133</sup> For non-interacting rods, the percolation threshold occurs near the transition between the semi-di-

lute and concentrated regimes, where the rod number density is roughly the reciprocal of the excluded volume of the rod,  $\nu_{\text{excl}}$ ,<sup>25,34,35</sup> which here can be approximated by  $\nu_{\text{excl}} \approx \pi^2 d/2$ , where  $d$  and  $\pi$  are as defined earlier. The threshold is thus predicted to be at a volume fraction  $\phi_1 \approx d/2$ . While valid for systems of non-interacting rods, this model as a limited success predicting the percolation-like behavior of strongly interacting nanotube systems. Attractive interactions can lower threshold concentrations when the particles assemble to form long chains. The simplest model for these attractive systems assumes that the limiting concentration at which continuous chains can form occurs near the transition between dilute and semi-dilute regimes, where the rotational motion of each rod is obstructed by the presence of other rods.<sup>36-38</sup> Here, the volume occupied by each rod is a sphere of diameter  $d$ , so  $\nu_0 \approx \pi^3/6$ , and the critical volume fraction is  $\phi_0 \approx 3d^2/2$ . The model predicts a significantly lower threshold than the excluded-volume picture described above, and provides a lower bound for the position of the threshold when the rods are distributed randomly. It is thus reasonable that the threshold should be observed in the semi-dilute regime between the two limiting cases described above.

While these models oversimplify the situation in our composites, they do give a range of concentrations where the threshold can be expected. If we approximate our laser-oven (HiPco) samples as homogeneous rod distributions with length  $516 \text{ nm}$  ( $167 \text{ nm}$ ) and diameter  $1.35 \text{ nm}$  ( $1.1 \text{ nm}$ ), then we can define limiting theoretical percolation thresholds using the simple models outlined above. The wavy and solid lines in Figure 3 correspond to dilute/semi-dilute and semi-dilute/concentrated transition points, respectively. Thresholds for all four sets of composites were observed in the semi-dilute regime, as expected in a system of attractive rods. The result is also consistent with rheological studies of surfactant-stabilized SWNTs in solution, where gelation percolation was observed in the semi-dilute regime.<sup>139</sup> The models also make quantitative predictions about the ratio of the HiPco threshold to the laser-oven threshold. The observed threshold ratio for our composites was  $1.7$  for non-sonicated samples and  $2.2$  for sonicated samples. If the samples are overlap-volume limited (i.e.,  $\nu_0$  limited), then the predicted ratio is  $6.5$ . If the samples are excluded-volume limited (i.e.,  $1/\nu_{\text{excl}}$  limited), then the observed ratios are predicted to be  $2.5$ . Although closer to the

**Table 1.** Observed thresholds, exponents, and predicted thresholds for the four data sets. All numbers are given in terms of SWNT volume fraction.

	Laser-oven		HiPco	
	Non-sonicated	Sonicated	Non-sonicated	Sonicated
Threshold volume fraction $\phi_c \times 10^5$	$5.2 \pm 1.9 / -0.5$	$10 \pm 2 / -1$	$8.5 \pm 1.0 / -0.9$	$23 \pm 2 / -2$
Best-fit exponent $\beta$	$2.7 \pm 0.4 / -0.8$	$1.6 \pm 0.5 / -0.6$	$3.1 \pm 1.2 / -1.7$	$3.2 \pm 0.5 / -0.6$
Dilute/semi-dilute transition $\phi_0$	$8 \times 10^{-58}$	$8.81 \times 10^{-58}$	$6.5 \times 10^{-58}$	$6.5 \times 10^{-58}$
Semi-dilute/concentrated transition $\phi_1$	$1.3 \times 10^{-58}$	$1.3 \times 10^{-58}$	$3.3 \times 10^{-58}$	$3.3 \times 10^{-58}$

latter[ratio,our observations do not agree with either model. Another potentially testable prediction is the percolation exponent,  $s$ . [The confidence intervals for our exponents were large and their best fits ranged from  $1.6(+0.5/-0.6)$  to  $3.2(+0.5/-0.6)$ . Computer models of conductivity percolation predict a critical exponent value<sup>[40]</sup> of 2. Other experimental studies of carbon nanotube composites have frequently reported values<sup>[5,9,13,28]</sup> between 1.3 and 2, while exponents of 3.1 were observed in disordered, short-carbon-fiber composites.<sup>[41]</sup>

In summary, we have developed a methodology to sparsely purify SWNTs into epoxy and we have investigated the electrical conductivity in these composites as a function of SWNT length, type, and dispersion homogeneity. All four varieties of our composites exhibited percolation-like thresholds in the semi-dilute concentration regime. The lowest thresholds were observed when the SWNTs were allowed to reaggregate, and these were significantly lower than have been previously reported for SWNTs in epoxy.

## Experimental

Nanotubes were obtained in raw form and purified according to procedures largely described in previous publications [42] and [43]. The suspensions were magnetically fractionated, reducing the magnetic-catalyst fraction to  $\leq 0.7$  wt.-% and then the nanotubes were annealed at  $1150^\circ\text{C}$ . A combination of X-ray and thermogravimetric analysis (TGA) measurements suggested that the resultant purified nanotubes contained  $>95$  wt.-% SWNTs and  $<5$  wt.-% carbon-devoid (amorphous carbon, graphite) impurities, in addition to the above-mentioned small quantities of catalyst particles. Details of the TGA and X-ray analyses are given in previous publications ([29] and [44], respectively). The purified nanotubes were dispersed using a low-power ultrasonic frequency sonicator (Cole-Parmer model 08849-00, 1 pint, 17 W) at concentrations of 0.004 wt.-% and 0.04 wt.-% in *N,N*-methylformamide (DMF). To characterize the dispersion, we deposited SWNTs onto an amorphous silicon wafer by dipping the wafer into the SWNT suspensions and then measured the height of the deposited nanotubes using atomic force microscopy. Figure 1g shows an AFM image of a wafer that was left in solution for 30 min; our quantitative dispersion data, however, were derived from similar images of wafers that were only briefly dipped into the solution, and therefore contained a much lower density of adsorbed SWNTs. The 0.004 wt.-% SWNT/DMF dispersion contained a mixture of isolated nanotubes ( $<10\%$ ) and small bundles ( $>90\%$ ), with mean height  $<6$  nm, whereas the 0.04 wt.-% SWNT-DMF dispersion contained many significantly larger bundles.

Our thermoset epoxy was Shell Epon 828 (Bisphenol-A, Miller-Stephenson, density:  $1.16\text{ g cm}^{-3}$ ) epoxy resin with EpiKure 3234 (crosslinker (Triethylenetetramine, Miller-Stephenson, density:  $0.98\text{ g cm}^{-3}$ ). The density of cured epoxy was found to be  $1.2 \pm 0.02\text{ g cm}^{-3}$ . We use the cured epoxy density along with the calculated value of  $1.4\text{ g cm}^{-3}$  for nanotube density [9] to convert from units of weight percent to volume fraction. For each SWNT-composite sample, 0.5 g of epoxy resin was placed in a low-power ultrasonic bath sonicator. The sonicator temperature was maintained at  $80^\circ\text{C}$ . SWNT/DMF suspension was added to the bath and sonicating epoxy resin with a glass syringe in 1 mL increments every 30 min, until the desired nanotube concentration was reached. The elevated sonication temperature reduced the viscosity of the epoxy resin; this step was necessary for effective sonication and fast DMF evaporation. The resultant sample was left in the sonicator for an additional 2–3 h to ensure complete evaporation of DMF. We then added 65  $\mu\text{L}$  of crosslinker to the sonicating SWNT/epoxy resin mixture. We stirred the mixture me-

chanically for two minutes, and then loaded it into a thin-walled cylindrical Teflon mold. Curing proceeded either under continued sonication or without, as described above. All samples were subsequently annealed in an oven at  $120^\circ\text{C}$  for two hours. Thus prepared, the samples were cut with a diamond saw into  $5.4\text{ mm} \times 2.5\text{ mm} \times 300\text{ }\mu\text{m}$  thick pieces, and the flat ends were polished on  $5\text{ }\mu\text{m}$  grain polishing paper.

For two-point measurements, the flat surfaces of the cylindrical composite samples were painted with conductive paint (product number 4929N, DuPont). For four-point measurements, the samples were further prepared by roughening the curved surface of the cylindrical samples and painting conductive rings around their circumference with a spacing of approximately 1 mm. Copper leads were attached to these electrodes with the same conductive paint. (See insets in Fig. 2.) Samples with conductive ties of less than  $1 \times 10^{-10}\text{ Scm}^{-1}$  were measured by an alternating-current two-point method that utilized capacitive decay curves to extract conductivity [45]. The measurement error for the conductivity was  $\leq 1\%$ , and the nanotube volume fraction was known to within 10%. The sensitivity limit of our apparatus was approximately  $1 \times 10^{-14}\text{ Scm}^{-1}$ , as indicated by the shaded gray areas in Figure 3. We confirm the conductivity was isotropic; conductive ties measured along three perpendicular axes were within 25% of one another. Weak aging effects were observed in our composites. After a period of two months, the conductivities of all samples were observed to decrease by approximately 50%. The conductivity recovered to 75%–100% of its original value after heating at  $110^\circ\text{C}$  for 1 h. To assess the possibility of ionic conduction through any remaining solvent, control samples were prepared that underwent the same processing with pure DMF in place of the SWNT/DMF dispersion. All of these control samples were insulating below the noise floor of the measurement.

Received: October 6, 2004  
Final version: February 1, 2005

- [1] S. Kirkpatrick, *Rev. Mod. Phys.* **47**, 45 (1975).
- [2] J. G. Smith, Jr., J. W. Connell, D. M. Delozier, P. T. Lillehei, K. A. Watson, Y. L. Jin, B. Zhou, Y. P. Sun, *Polymer* **2004**, 45 (2004).
- [3] N. S. Xu, Z. S. Wu, S. Z. Deng, J. Chen, *J. Vac. Sci. Technol. B* **2001**, 19, 1370.
- [4] Q. H. Wang, A. A. Setlur, J. M. Lauerhaas, J. Y. Dai, E. W. Seelig, R. P. H. Chang, *Appl. Phys. Lett.* **1998**, 72, 2912.
- [5] B. Kim, J. Lee, I. Yu, *J. Appl. Phys.* **2003**, 94, 6724.
- [6] M. J. Biercuk, M. C. Llaguno, M. Radosavljevic, J. K. Hyun, A. T. Johnson, J. E. Fischer, *Appl. Phys. Lett.* **2002**, 81, 2767.
- [7] C. Seoul, Y. T. Kim, C. K. Baek, *J. Polym. Sci., Part B: Polym. Phys.* **2003**, 41, 1572.
- [8] Z. Ounaies, C. Park, K. E. Wise, E. J. Siochi, J. S. Harrison, *Compos. Sci. Technol.* **2003**, 63, 1637.
- [9] C. Park, Z. Ounaies, K. A. Watson, R. E. Coffey, J. Smith, Jr., S. E. Lowther, J. W. Connell, E. J. Siochi, J. S. Harrison, T. L. St. Clair, *Chem. Phys. Lett.* **2002**, 364, 303.
- [10] E. J. Ymakis, I. Alexandou, G. A. J. Amarantunga, *Synth. Met.* **2002**, 127, 59.
- [11] J. E. Huang, X. H. Li, J. C. Xu, H. L. Li, *Carbon* **2003**, 41, 2731.
- [12] T. V. Sreekumar, T. Liu, B. G. Min, H. Guo, S. Kumar, R. H. Hauge, R. E. Smalley, *Adv. Mater.* **2004**, 16, 58.
- [13] R. Ramasubramanian, J. Chen, H. Liu, *Appl. Phys. Lett.* **2003**, 83, 2928.
- [14] R. Hagenmueller, H. H. Gommans, A. G. Rinzler, J. E. Fischer, K. I. Winey, *Chem. Phys. Lett.* **2000**, 330, 219.
- [15] F. Du, J. E. Fischer, K. I. Winey, *J. Polym. Sci., Part B: Polym. Phys.* **2003**, 41, 3333.
- [16] J. M. Benoit, B. Corraze, O. Chauvet, *Phys. Rev. B* **2002**, 65, 241405(R).
- [17] H. J. Barraza, F. Pompeo, E. A. O'Rear, D. E. Resasco, *Nanotechnology* **2002**, 13, 797.

- [18] Y. Lin, B. Zhou, K. A. S. Fernando, P. Liu, L. F. Allard, Y. P. Sun, *Macromolecules* **2003**, *36*, 7199.
- [19] J. Zhu, J. Kim, H. Peng, J. L. Margrave, V. N. K. [abash]esku, E. V. Barrera, *Nanocett. c* **2003**, *3*, 1107.
- [20] O. Regev, P. N. B. ElKati, J. Loos, C. E. Koning, *AdvancMater. c* **2004**, *16*, 248.
- [21] A. Nogales, G. B{oz}a, Z. Roslaniec, K. Schulte, I. {S}ics, B. S. Hsiao, A. Sanz, M. C. Garc{a}a-Gut{e}rrez, D. R. Rueda, C. Domingo, T. A. Ezquerro, *Macromolecules* **2004**, *37*, 7669.
- [22] J. C. Grunlan, A. R. Mehrabi, M. V. Bannon, J. L. Bahr, *AdvancMater. c* **2004**, *16*, 150.
- [23] A. Allaoui, S. Bai, H. M. Cheng, J. B. Bai, *Compos.cSci.cTechnol. c* **2002**, *62*, 1993.
- [24] J. Sandler, M. S. P. Shaffer, T. Prasse, W. Bauhofer, K. Schulte, A. H. Wndle, *Polymer* **1999**, *40*, 5967.
- [25] I. Balberg, N. Binenbaum, N. Wagner, *Phys. Rev. Lett.* **1984**, *52*, 1465.
- [26] R. Schueler, J. Petermann, K. Schulte, H. P. Wentzel, *J. Appl. Polym. Sci.* **1997**, *63*, 1741.
- [27] S.-P. Rwei, F.-H. Ku, K.-C. Cheng, *ColloidePolym.cSci.c* **2002**, *280*, 1110.
- [28] J. K. W. Sandler, J. E. Kirk, I. A. Kinloch, M. S. P. Shaffer, A. H. Wndle, *Polymer* **2003**, *44*, 5893.
- [29] M. F. Islam, D. E. Mlikie, C. L. Kane, A. G. Yo, J. M. Kkawa, *Phys. Rev. Lett.* **2004**, *93*, 037404.
- [30] M. F. Islam, E. Rojas, D. M. Bergey, A. T. Johnson, A. G. Yodh, *Nanocett. c* **2003**, *3*, 269.
- [31] M. S. P. Shaffer, A. H. Wndle, *AdvancMater. c* **1999**, *11*, 937.
- [32] W. Zhou, M. F. Islam, H. Wang, D. L. Ho, A. G. Yodh, K. I. Wney, J. E. Fscher, *Chem. Phys. Lett.* **2004**, *384*, 185.
- [33] M. Doi, S. F. Edwards, *The Theory of Polymer Dynamics*, 1st ed., International Series on Monographs of Physics, Vol. 73, Oxford Science Publications, Oxford, UK **1986**.
- [34] I. Balberg, C. H. Anderson, S. Alexander, N. Wagner, *Phys. Rev. B* **1984**, *30*, 3933.
- [35] A. L. Bug, S. A. Safran, I. Webman, *Phys. Rev. Lett.* **1985**, *54*, 1412.
- [36] F. Carmona, F. Barreau, P. Delhaes, R. Canet, *J. Phys. Chem.* **1980**, *41*, L531.
- [37] F. Carmona, P. Prudhon, F. Barreau, *Solid State Commun.* **1984**, *51*, 255.
- [38] A. P. Philipse, A. M. Wrenga, *angmuir* **1998**, *14*, 49.
- [39] L. A. Hough, M. F. Islam, P. A. Janmey, A. G. Yo, *Phys. Rev. Lett.* **2004**, *93*, 168102.
- [40] S. P. Obukhov, *Phys. Rev. Lett.* **1995**, *74*, 4472.
- [41] C. V. Inches, L. Salome, C. Coulon, F. Carmona, *J. Phys. Chem.* **1990**, *51*, 2505.
- [42] A. G. Rinzler, J. Liu, H. Dai, P. Nikolaev, C. B. Huffman, F. J. Rodriguez-Marcias, P. J. Boul, A. H. Lu, D. Heyman, D. T. Colbert, R. S. Lee, J. E. Fscher, A. M. Rao, P. C. Eklund, R. E. Smalley, *Appl. Phys. Lett.* **1998**, *72*, 29.
- [43] J. H. Hafner, M. J. Bronikowski, B. R. Azamian, P. N. Nikolaev, A. G. Rinzler, D. T. Colbert, K. A. Smith, R. E. Smalley, *Chem. Phys. Lett.* **1998**, *296*, 195.
- [44] W. Zhou, Y. H. Ooi, R. Russo, P. Papanek, D. E. Luzzi, J. E. Fscher, M. J. Bronikowski, P. A. Willis, R. E. Smalley, *Chem. Phys. Lett.* **2001**, *350*, 6.
- [45] A. Daire, *Keithley white paper, "Improving the Repeatability of Ultra-High Resistance and Resistivity Measurements."* **2001**.

## Phthalocyanine Composites as High-Mobility Semiconductors for Organic Thin-Film Transistors\*\*

By Jianc Zhang, Haiboc Wang, Xuanjun Yan, Junc Wang, Jianwuc Shi, and Donghang Yan\*

There is a growing research effort in organic thin-film transistors (OTFTs) because organic semiconductors possess numerous advantages, including large-area coverage, easy processing, good compatibility with a variety of substrates including flexible plastics, and great opportunities for structural modification.<sup>[1–4]</sup> A lot of research has been carried out by efforts to synthesize new materials with promising properties, such as high mobilities and high on/off ratios.<sup>[5–7]</sup> Semiconducting materials with high performance can also be formed by the incorporation of two different organic materials.<sup>[8]</sup> However, composites of organic semiconductors have scarcely been investigated in OTFTs.<sup>[9,10]</sup> Also, the mobility of the composites are relatively low.

Phthalocyanines (Pcs) are a large family of conjugated molecules with high chemical and thermal stabilities.<sup>[11]</sup> They exhibit outstanding optical and electrical properties of these materials open up a wide range of applications, including electrochemical devices, optical switches, data-storage media, gas sensors, solar cells, and OTFTs.<sup>[12–17]</sup> Our results on OTFTs using source and drain electrodes sandwiched between copper phthalocyanine (CuPc) and cobalt phthalocyanine (CoPc) layers reveal that composites of the two Pcs have different characteristics than the pure materials.<sup>[18]</sup> A composite of CuPc and nickel phthalocyanine (NiPc), CuPc–NiPc, synthesized as the active layer in an OTFT in this article. An OTFT in top-contact configuration is schematically depicted in Figure 1. CuPc and NiPc films have been deposited to compare the structures of the materials.

Representative transfer characteristics are shown in Figure 1 for OTFTs based on CuPc–NiPc (9:1 w/w) films. From the square root of the drain current ( $I_D^{1/2}$ ) vs. gate voltage ( $V_G$ ) curve at a fixed drain-source voltage ( $V_D$ ) of  $-40$  V, the field-effect mobility ( $\mu$ ) in the saturation regime for the CuPc–NiPc (9:1) device is estimated to be  $0.050 \text{ m}^2 \text{V}^{-1} \text{s}^{-1}$ . The corresponding linear regime mobility is  $0.025 \text{ m}^2 \text{V}^{-1} \text{s}^{-1}$ . The reduction of linear regime mobility relative to the saturation-regime value may be attributed to traps in the organic

\*Jiang Prof. Dr. J. Zhang, H. Wang, X. Yan, J. Wang, J. Shi  
State Key Laboratory of Polymer Physics and Chemistry  
Changchun Institute of Applied Chemistry  
The Chinese Academy of Sciences  
5625 Renmin St., Changchun 30022 (P. R. China)  
E-mail: andh@ciac.jl.cn

\*\*This financial support by the National Science Foundation of China (90301008, 820025413, 820474064) and the Special Funds for Major State Basic Research Projects (2002CB613404) is gratefully acknowledged.